PISTON
Journal of Technical Engineering:

Crashworthiness Evaluation of Side Sill Structures under Aluminum Alloy Variation and Multi-Cell Configuration Using the Finite Element Method

Rafly Aura Permana Hervianto[1,a)], Mochammad Avrieza Havies Aravy[1], Nabila Putri Ramadahni[1], Vias Diana Ayu Asari[1], Noval Syafiq Raihan[1], R. Arief Novianto[1], Ahmad Ashari[1]

[1]*Automotive Engineering Technology, Polytechnic of Road Transportation Safety, Tegal, Indonesia*

E-mail: [a)] raflyhervianto07@gmail.com

Received: April 28, 2026 *Revision: July 04, 2026* *Accepted: July 23, 2026*

Abstract: The high-fatality rate of traffic accidents, particularly in side collisions, indicates that current vehicle safety systems are not fully effective in protecting passengers. This issue becomes more critical in electric vehicles due to the potential risk of battery damage. This study aims to improve the crashworthiness of side sill structures through the selection of aluminum alloy materials and multi-cell design configurations to enhance energy absorption and maintain cabin integrity. The materials investigated include Aluminum 6061-T6, Aluminum 6082-T6, and Aluminum 7075-T6. The methodology involves geometric modeling using SolidWorks 2022 and finite element-based impact simulations using ANSYS Explicit Dynamics 2024 R2 at an impact speed of 60 km/h. The evaluation parameters include von Mises stress, energy absorption, and total deformation. The results show that Aluminum 7075-T6 exhibits the best performance, with a maximum stress of 499.84 MPa, an energy absorption capacity of 3.46×10^5 J, and a deformation of 18.253 mm, which remains progressive and localized, thereby maintaining structural integrity. In comparison, Aluminum 6061-T6 and 6082-T6 show lower stress values with relatively similar deformation patterns. Overall, the combination of multi-cell design and Aluminum 7075-T6 provides the best crashworthiness performance in enhancing energy absorption and cabin protection in side-impact scenarios.

Keywords: crashworthiness; side sill; finite element method; aluminum alloys; multi-cell structure; energy absorption.

Abstrak: *Tingginya angka fatalitas kecelakaan lalu lintas, khususnya pada tabrakan samping, menunjukkan bahwa sistem keselamatan kendaraan saat ini belum sepenuhnya efektif dalam melindungi penumpang. Permasalahan ini menjadi semakin kritis pada kendaraan listrik akibat potensi risiko kerusakan baterai. Penelitian ini bertujuan untuk meningkatkan crashworthiness struktur side sill melalui pemilihan material paduan aluminium dan konfigurasi desain multi-cell guna meningkatkan penyerapan energi serta menjaga integritas kabin. Material yang dikaji meliputi Aluminium 6061-T6, Aluminium 6082-T6, dan Aluminium 7075-T6. Metodologi yang digunakan mencakup pemodelan geometri menggunakan SolidWorks 2022 serta simulasi impak berbasis metode elemen hingga menggunakan ANSYS Explicit Dynamics 2024 R2 pada kecepatan tumbukan 60 km/jam. Parameter evaluasi meliputi tegangan von Mises, penyerapan energi, dan deformasi total. Hasil penelitian menunjukkan bahwa Aluminium 7075-T6 memiliki performa terbaik, dengan tegangan maksimum sebesar 499,84 MPa, kapasitas penyerapan energi sebesar* 3.46×10^5 *J, serta deformasi sebesar 18,253 mm yang bersifat progresif dan terlokalisasi sehingga mampu mempertahankan integritas struktur. Sebagai perbandingan, Aluminium 6061-T6 dan 6082-T6 menunjukkan nilai tegangan yang lebih rendah dengan pola deformasi yang relatif serupa. Secara keseluruhan, kombinasi desain multi-cell dan Aluminium 7075-T6 memberikan performa crashworthiness terbaik dalam meningkatkan penyerapan energi dan perlindungan kabin pada skenario tabrakan samping.*

Kata kunci: *crashworthiness; side sill; metode elemen hingga; paduan aluminium; struktur multi-sel; penyerapan energi.*

INTRODUCTION

The achievement of road transportation safety standards in Indonesia is currently in a state of high urgency due to the uncontrolled escalation of accident fatalities. Statistical data confirm the critical fatality rate,

ISSN: 2541-3511 © 2026 The Author(s). This is an open access article under the Creative Commons Attribution-NonCommercial 4.0 International License (https://creativecommons.org/licenses/by-nc/4.0/).

with an average of three to four lives lost every hour due to incidents on the highway. The dominance of human factors by more than 80 percent, especially high-speed behavior, indicates systemic failures in mitigating driving risks. In addition to the loss of life, massive economic and social impacts have the potential to trigger new poverty vulnerabilities for victims' families [1]. Therefore, strengthening vehicle crashworthiness through advanced structural analysis is a crucial step to mitigate these risks.

The side-pole collision scenario is one of the most critical threats to the structural integrity of a vehicle due to the highly centralized area of contact. The limitation of the crumple zone on the side of the vehicle causes the absorption of kinetic energy to be ineffective compared to a frontal collision [2], [3]. The impact force is directed to vital components such as the B-pillar, so the risk of life-threatening cabin intrusion is very high. This phenomenon is increasingly complex in electric vehicles because the potential for damage to the battery pack can trigger secondary hazards in the form of fire or electrical failure [4], [5]. Therefore, an in-depth analysis of the dynamics of side impacts is a fundamental parameter in evaluating the effectiveness of the vehicle safety system as a whole [6].

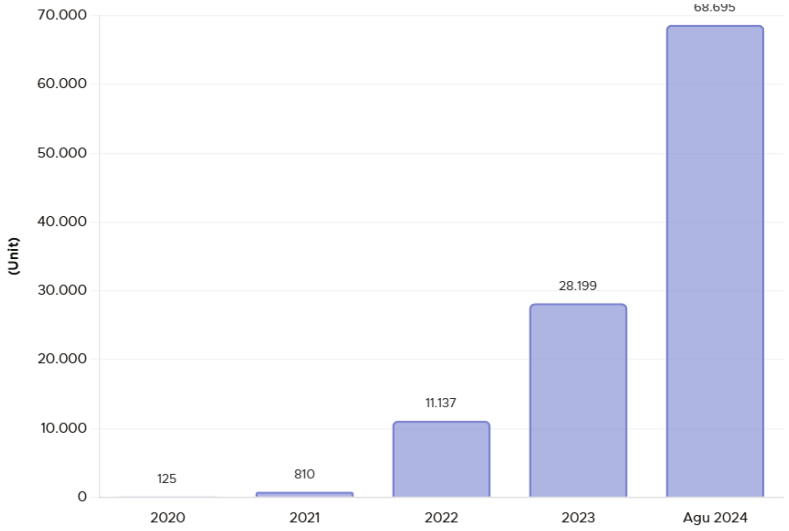

Figure 1. Growth in the Number of 4-Wheeled EVs in Indonesia [7].

The side sill structure plays a crucial role as the main load path as well as a kinetic energy absorber to maintain the integrity of the electric vehicle during a side impact. The design of this component functions strategically in dissipating impact energy to prevent cabin intrusion and protect the battery module from fatal mechanical damage [8]. The implementation of the Euro NCAP 135 (UN R135) regulation tests this durability through a simulation of a 254 mm diameter rigid pole collision at a speed of 32 km/h. The FMVSS 214 standard complements the test parameters with an angle of impact of 75 degrees to ensure the effectiveness of passenger protection in extreme collision conditions [9], [10].

Thus, improving side sill design based on global regulatory standards is the main foundation for enhancing vehicle collision feasibility before conducting a more specific material selection analysis. A multi-cell side sill in electric vehicles is a strategic innovation to maximize crashworthiness while protecting the battery system. This structure has a major advantage in energy dissipation because the addition of a core layer or cell increases the number of plastic hinges, which are able to increase specific energy absorption (SEA) by 30–60% compared to single-cell profiles [11]. The use of layered designs such as honeycomb sandwich structures is able to create a gradual deformation mechanism that is effective in distributing the impact load evenly. These technical configurations proactively minimize intrusion into the battery compartment to prevent the risk of thermal runaway or harmful electrical failure [12], [13]. Through these various structural advantages, the use of a layered side sill is a crucial solution in ensuring the operational safety of electric vehicles.

The material selection between the 6061-T6, 6082-T6, and 7075-T6 aluminum series results in a significant variation in mechanical performance regarding the impact characteristics of side sill components. Based on literature studies and material specification data, 6061-T6 aluminum exhibits better energy absorption stability and ductility than 7075-T6 when facing large-scale impact loads [14]. Meanwhile, 6082-T6 aluminum has approximately 17% higher tensile strength than 6061-T6, making it more effective for extrusion profiles that require high rigidity [15]. On the other hand, 7075-T6 aluminum offers a very high strength-to-weight ratio with a yield strength above 500 MPa, yet it has a higher brittle failure tendency under critical impact loads [16]. Therefore, this comparison of mechanical properties is used as a basis for material selection before further

structural analysis. This study aims to evaluate and recommend the type of aluminum alloy with the most superior performance to be applied to the energy-absorbing structure of electric vehicles.

This study offers a novel contribution through a specific comparative analysis of Aluminum 6061-T6, 6082-T6, and 7075-T6, building on previous research that relied only on the assumption of elasto-plastic bilinear materials. An in-depth analysis was carried out to map the optimal balance between tensile strength and impact energy absorption capacity in each of the mechanical characteristics of the material. This empirical approach in material selection is projected to significantly improve the crashworthiness performance of the structure compared to the use of standard, generalized material models. The results of this evaluation will provide the best material recommendations, serving as a crucial foundation for the structural design improvement process in the next stage of simulation.

METHODS

Research Flowchart

This numerical research procedure was systematically designed to ensure that all stages of the simulation are consistent and verifiable. The process began with a literature review to establish the theoretical foundation, modeling methods, and valid references related to the crashworthiness analysis of side sill structures. Next, a geometric model was developed to realistically represent the components before being implemented into the simulation environment. The next stage involves discretizing the model through a meshing process, selecting elements appropriate for the characteristics of thin-plate structures to accurately capture deformation responses. Afterward, the parameters for explicit dynamic analysis are defined, including boundary conditions, impact loading, and contact interactions between components. To improve the reliability of the results, a mesh convergence test was conducted to ensure that variations in element size did not significantly affect the simulation output. The stabilized model was then compared with a reference study as a form of preliminary validation before the final results were processed and visualized for further analysis.

The side sill component geometry was modeled in three dimensions using SolidWorks 2022 software to accurately represent the vehicle's actual structure. The model was designed to capture the geometric characteristics that influence stress distribution during a side impact. In this study, the materials analyzed are three aluminum alloy variants, namely Al 6061-T6, Al 6082-T6, and Al 7075-T6, each of which differs in chemical composition and mechanical response to plastic deformation. Prior studies on 6xxx- and 7xxx-series aluminum alloys report that these differences translate into markedly different impact energy-absorption behavior, with Al 7075-T6 offering higher yield strength but comparatively lower ductility relative to the 6xxx series [14]. Consistent with this, Al 7075-T6 has been reported to provide superior collision resistance when applied to automotive body structural components such as center pillars, despite its slightly higher density [17].

The behavior of materials under high-speed dynamic loading cannot be assumed to be linear; therefore, a constitutive approach capable of representing the influence of strain rate is required. Consequently, the Johnson–Cook plasticity model was used to describe the stress-strain response of the materials under nonlinear plastic deformation conditions [18], [19]. This formulation integrates the effects of strain hardening, strain rate sensitivity, and thermal softening [20]. The flow-stress model is expressed as:

$$\sigma_y = \left[A + B(\varepsilon_p)^n\right]\left[1 + C\ln\left(\dot{\varepsilon}^*\right)\right]\left[1 - \left(T^*\right)^m\right] \quad (1)$$

where σ_y is the yield stress, A is the initial yield strength of the material, B is the strain hardening constant, and n is the strain hardening exponent [21], [22]. The parameter C represents the strain rate sensitivity coefficient, while $\dot{\varepsilon}^*$ is the dimensionless plastic strain rate. The normalized temperature parameter (T^*) raised to the power of the thermal softening exponent (m) accounts for the reduction in material strength caused by thermal softening during impact loading. Structural failure was modeled using the Equivalent Plastic Strain (EPS) criterion, in which elements were automatically eroded once the equivalent plastic strain exceeded the critical failure limit defined for the material.

The side sill structure was discretized in ANSYS Explicit Dynamics 2024 R2 using Belytschko-Lin-Tsay shell elements, which are widely employed in explicit crashworthiness analyses because of their computational efficiency and numerical stability for thin-walled structures undergoing large deformation [23]. To achieve an appropriate balance between solution accuracy and computational cost, adaptive mesh refinement was adopted. A local element size of 5 mm was applied to the primary impact region to accurately capture stress concentrations and plastic deformation, whereas a global element size of 15 mm was assigned to the remaining structural regions. Mesh quality was verified through a mesh convergence study by gradually refining the element size while monitoring the von Mises stress distribution and internal energy. Numerical convergence was considered achieved

when successive mesh refinements produced variations of less than 5%, indicating that the selected mesh density provided stable and reliable simulation results [24].

A nonlinear body-to-body frictional contact formulation was employed to simulate the interaction between the impactor and the side sill during lateral impact loading. Self-contact was also activated to prevent numerical penetration between structural components and to accurately represent local folding and wall instability during large plastic deformation. Dry contact conditions were assumed with a dynamic friction coefficient of 0.3, representing the interaction between aluminum and steel under impact loading. The impactor was modeled as a rigid body to ensure that the initial kinetic energy was transferred directly to the side sill without deformation of the striking component. A translational velocity of 16.67 m/s (60 km/h) was applied along the impact direction to represent a passenger vehicle side-impact collision. Fixed support constraints were imposed at the chassis attachment locations to represent the structural stiffness of the vehicle body while allowing deformation to be concentrated within the side sill region.

The stability of the explicit dynamic simulation was assessed by monitoring the hourglass energy and artificial energy throughout the analysis. Both parameters were maintained below 5% of the total internal energy to minimize numerical artifacts and ensure that the predicted structural response was governed by physical deformation mechanisms rather than numerical instability. The developed finite element model was validated against experimental results reported in the literature [25]. Validation was performed by comparing the force-displacement response, including the peak load, progressive deformation behavior, and energy absorption characteristics. In addition, the predicted failure mode was qualitatively compared with experimental observations to verify the consistency of the deformation patterns. The agreement between the numerical and experimental results was quantified using the percentage error, confirming that the developed model provides sufficient accuracy for the crashworthiness evaluation of the side sill structure [26].

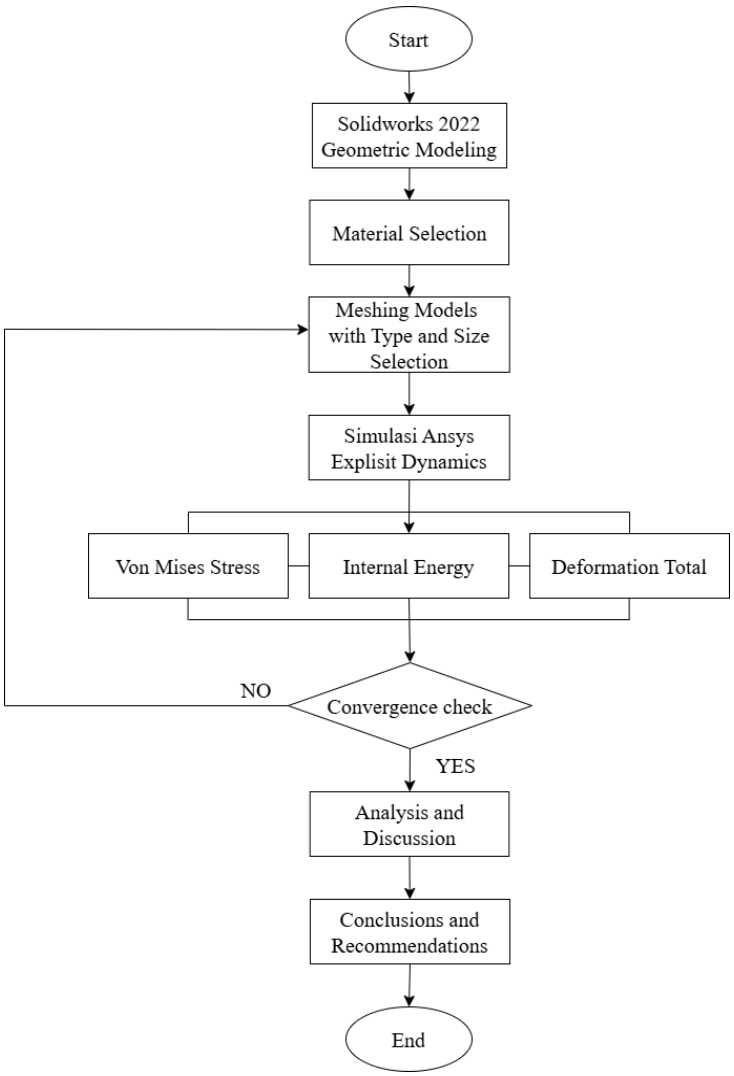

Figure 2. Research flowchart of side sill with ANSYS Explicit Dynamics

Modeling

The side sill geometry was modeled as an elongated profile with a total length of 2000 mm and a cross-sectional height of 207 mm. The three-dimensional geometric model was developed using SolidWorks 2022 and subsequently imported into ANSYS Explicit Dynamics 2024 R2 for crashworthiness analysis. This structural configuration accurately reflects the actual vehicle underbody components, particularly in regions responsible for load transfer and energy absorption during side-impact events.

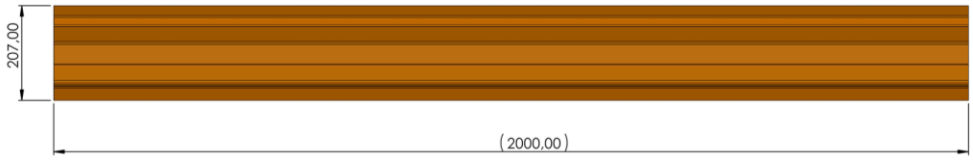

Figure 3. Front view of side sill

The side sill model investigated in this study is illustrated in Figure 4. The structure consists of two main components: the inner sill section and the front section, which are joined through a welding process to form a continuous load-bearing member. The inner sill features a rectangular cross-section reinforced with flanges to improve structural stiffness, while the front section protrudes outward and functions as the primary energy-absorbing region during the initial stage of lateral impact. Both components are designed with varying wall thicknesses according to their structural functions.

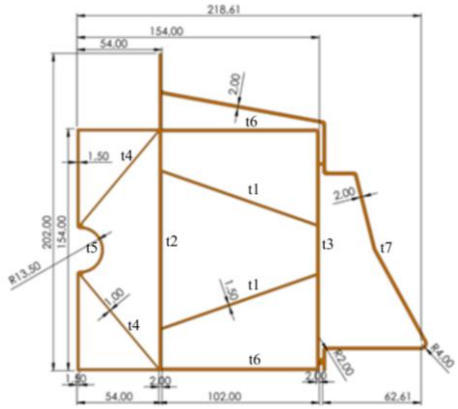

(a)

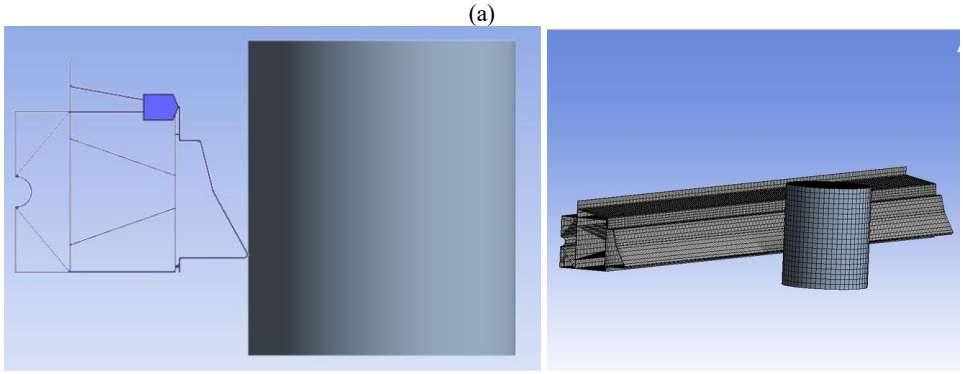

(b) (c)

Figure 4. (a) geometry values, (b) boundary conditions of side sill, (c) meshed area of side sill

Appropriate boundary conditions were applied to represent the attachment of the side sill to the vehicle body, thereby enabling a realistic prediction of structural deformation behavior under impact loading [21]. Figure 4 presents the detailed geometry, boundary conditions, and mesh discretization adopted in the finite element model. The generated mesh satisfies the numerical convergence requirements while minimizing excessive element distortion, thereby improving the reliability and stability of the simulation results.

The crash simulation employed an initial impact velocity of 60 km/h, representing a moderate side-impact collision scenario [22], [23]. This impact speed was selected based on empirical evidence indicating that most lateral vehicle collisions occur within this velocity range. Furthermore, statistical analyses by Radzi et al. reported an average collision speed of approximately 58.96 km/h for vehicles with an average mass of 1453.08 kg, confirming that the selected loading condition closely represents real-world traffic accident scenarios [24].

The results of their study also showed that passenger injury and fatality rates tend to be significantly higher in collisions at speeds above 50 km/h. Therefore, this velocity serves as a valid and significant test parameter to analyze the structural response of the side sill.

In the explicit dynamic simulation, the impactor was modeled as a rigid body to eliminate impactor deformation and ensure that the kinetic energy was transferred directly to the side sill structure. An equivalent impactor mass of 1453.08 kg was selected to generate a representative lateral impact load capable of producing realistic plastic deformation and progressive damage while maintaining numerical stability throughout the analysis.

Table 1. Wall thickness range and step size

Thickness Variable	Initial Value (mm)	Step Size (mm)
t_1	1.5	0.1
t_2	2.0	0.2
t_3	2.0	0.2
t_4	1.0	0.1
t_5	1.5	0.1
t_6	2.0	0.2
t_7	2.0	0.2

This study employs a structured parametric approach to investigate the influence of wall thickness variations across critical side sill zones on crashworthiness performance. The structural design parameters are defined as a design vector T, consisting of the wall thickness variables assigned to each critical structural region:

$$T = [t_1, t_2, t_3, t_4, t_5, t_6, t_7\ ]^T \quad (2)$$

These variables are defined within practical manufacturing and design constraints to ensure feasible structural configurations. A series of predefined thickness combinations is generated by systematically varying the wall thickness within the ranges and fixed step sizes specified in Table 1. Each design configuration is analyzed independently using ANSYS Explicit Dynamics under identical lateral impact loading and boundary conditions. This enables a systematic assessment of the relationship between local thickness variations and key crashworthiness indicators, such as stress distribution, plastic deformation, and energy absorption.

The optimization framework follows a multi-objective optimization approach. The overall objective function, $O(T)$, is formulated by combining multiple crashworthiness objectives into a single optimization function using the weighted-sum method. The optimization simultaneously aims to maximize energy absorption while minimizing the mass of the side sill. The multi-objective function is expressed as:

$$O(T) = w_1 \cdot f_1(T) + w_2 \cdot f_2(T) \quad (3)$$

where $O(T)$ represents the multi-objective functions value for a given design vector, while $f_1(T)$ and $f_2(T)$ represent the individual objective functions for energy absorption and structural mass, respectively.

To prioritize crashworthiness performance, the weighting factors were assigned as $w_1 = 1.0$ for the energy absorption objective and $w_2 = -0.5$ for the mass objective. This weighting scheme places greater emphasis on maximizing energy absorption while still accounting for mass reduction. Consequently, the optimization framework seeks to minimize the deviation between the achieved and target energy absorption values while reducing the total mass of the side sill as much as possible.

Materials

Table 2. Material properties

Material	Density (kg/m^3)	Young's Modulus (GPa)	Yield Strength (MPa)	Ultimate Strength (MPa)	Poisson's Ratio
Aluminum 6061-T6	2700	69	276	310	0.33
Aluminum 6082-T6	2700	70	260	310	0.33
Aluminum 7075-T6	2810	71	503	572	0.33

The mechanical characteristics of various material candidates for the side sill structure are summarized in Table 2. This study evaluates three types of 6xxx and 7xxx series aluminum alloys, namely Aluminum 6061-T6, Aluminum 6082-T6, and Aluminum 7075-T6, to determine the material configuration with the best energy absorption performance. As shown in the data, Aluminum 7075-T6 exhibits the most superior mechanical specifications compared to the other variants. Although this material has a slightly higher density of 2810 kg/m^3, it offers a significantly higher yield strength of 503 MPa and a maximum ultimate strength of 572 MPa. The Young's modulus of 71 GPa in this material indicates higher structural rigidity, which is crucial for maintaining the integrity of the cabin space in the event of a lateral impact.

In comparison, Aluminum 6061-T6 and 6082-T6 have an identical density of 2700 kg/m^3 and a uniform Poisson's ratio of 0.33. Although Aluminum 6061-T6 is widely utilized due to its optimal balance between strength and manufacturability with a yield strength of 276 MPa, Aluminum 6082-T6 offers a comparable alternative with a slightly lower yield strength of 260 MPa, while maintaining the same ultimate strength of 310 MPa. The selection of materials in this simulation heavily accounts for the strength-to-weight ratio. The implementation of Aluminum 7075-T6 in the side sill structural modeling is projected to provide superior deformation resistance at an impact speed of 60 km/h, given that its load absorption capacity far exceeds that of the 6xxx-series aluminum alloys under extreme dynamic loading conditions.

RESULTS AND DISCUSSION

Equivalent von Mises Stress Analysis

The simulation results show that the three aluminum materials tested exhibited a relatively consistent response pattern characterized by local deformation in the impact contact zone, with a gradual collapse mechanism in the multi-cell structure. In the Al 7075-T6 material, the maximum stress value reached approximately 499 MPa, which numerically approaches the material's yield strength. This condition indicates that the material is operating at a high strength utilization level; however, this does not necessarily indicate superior performance. Rather, it is important to determine whether this condition is accompanied by deformation stability without the occurrence of complete structural failure.

From a deformation perspective, all materials exhibit values within a relatively narrow range, specifically around 18 mm. This very small difference indicates that the multi-cell geometry plays a dominant role in controlling the deformation pattern compared to material variations alone. The deformation that occurs is progressive and localized to the impact area, so there is no significant intrusion into the passenger compartment. This characteristic is more relevant for evaluating passive safety performance rather than simply comparing maximum stress values.

A more representative evaluation is obtained from energy absorption capacity. Simulation results show that Al 7075-T6 has the highest energy absorption capacity, followed by Al 6082-T6 and Al 6061-T6. This difference indicates that materials with higher strength tend to maintain a more effective plastic response under dynamic loading conditions, resulting in greater energy dissipation during the deformation process. However, this increase in energy absorption must be considered in conjunction with deformation stability; it should not stand alone as the sole performance indicator. Overall, crashworthiness performance is not determined by a single parameter but rather by a combination of structural collapse stability, progressive deformation patterns, and energy dissipation capability. In this context, Al 7075-T6 demonstrates the best overall performance because it is capable of maintaining structural integrity while still providing the highest energy absorption capacity, with no indication of global failure in a 60 km/h lateral impact scenario. Thus, material evaluation is conducted comprehensively based on energy response and deformation mechanisms, rather than solely on the magnitude of the stresses reached.

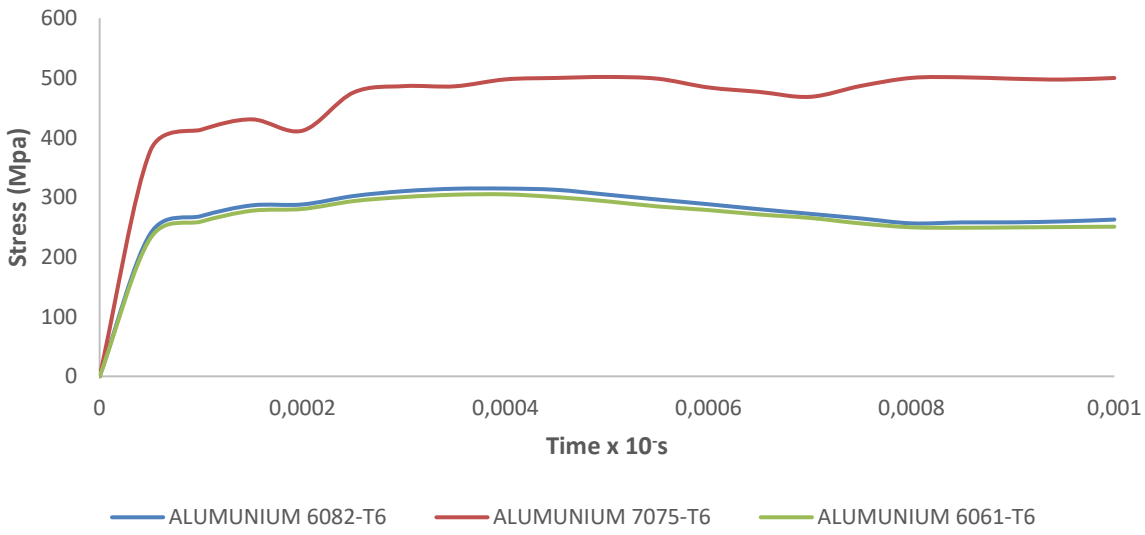

Figure 5. Equivalent von mises stress under side impact loading

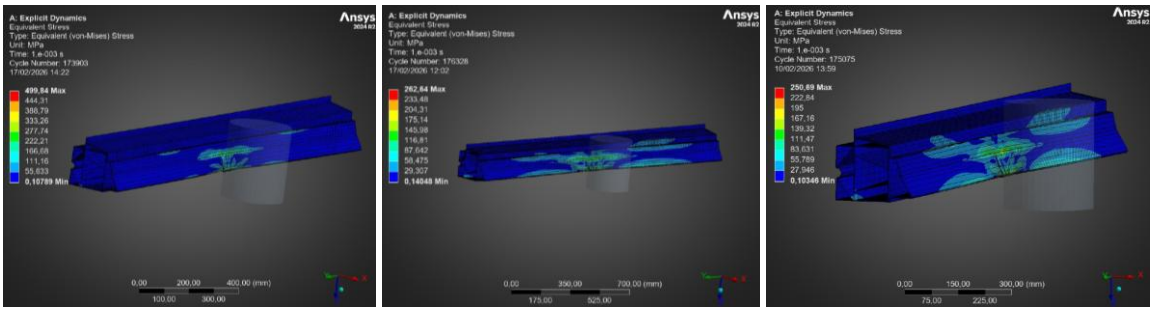

(a) (b) (c)

Figure 6. Comparison of von Mises stress distribution at 60 km/h: (a) Al 7075-T6, (b) Al 6082-T6, and (c) Al 6061-T6

The simulation results show that Al 7075-T6 reaches a maximum stress of approximately 499 MPa, which is close to its yield strength. This condition indicates that the material is in the active plastic phase during the impact process, which is precisely what is expected in an energy-absorbing structure because it allows for energy dissipation through controlled plastic deformation. However, the more relevant key indicators remain the stability of progressive deformation and the structure's ability to maintain integrity without experiencing global failure. In contrast, Al 6082-T6 and Al 6061-T6 exhibit lower stress values, approximately 262 MPa and 250 MPa, respectively.

This lower value cannot be directly interpreted as indicating lower performance or greater safety, as lower stress may indicate a different load distribution as well as varying plastic responses in the energy absorption mechanism. Therefore, the conclusion that the 7xxx series provides a greater safety margin needs to be reevaluated within a more comprehensive analytical framework. The safety margin in impact studies is determined not only by the margin relative to the yield stress, but also by how kinetic energy is converted into deformation energy in a stable manner, without causing sudden structural failure or loss of overall integrity. Therefore, material performance assessment should be based on a combination of deformation response, collapse stability, and energy absorption capacity, rather than solely on the maximum stress value achieved.

Deformation Characteristics and Structural Integrity

The simulation results show that the structural response of the side sill is dominated by local deformation in the impact contact zone, exhibiting characteristics of progressive collapse, which indicates the presence of a controlled energy dissipation mechanism. The localized damage distribution in the side sill area indicates that the impact energy is absorbed gradually through plastic buckling without causing failure to propagate to the vehicle's main structure. Thus, the integrity of the interior zone is maintained within deformation limits that remain within the lateral load-bearing structural area, thereby minimizing the potential for intrusion into the passenger compartment. However, interpreting performance based solely on a visual description of deformation patterns is insufficient; it must be linked to quantitative indicators such as intrusion depth, the evolution of deformation over time, and energy absorption capacity during the impact phase. This approach provides a more comprehensive picture for assessing the effectiveness of structural designs against lateral impact loads under real-world conditions.

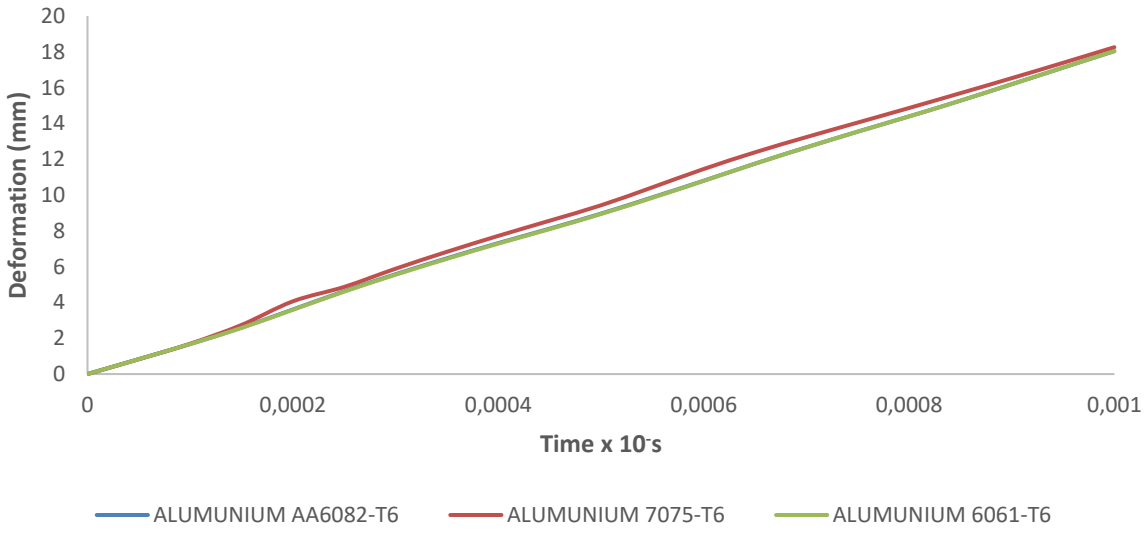

Figure 7. Total structural deformation under side impact

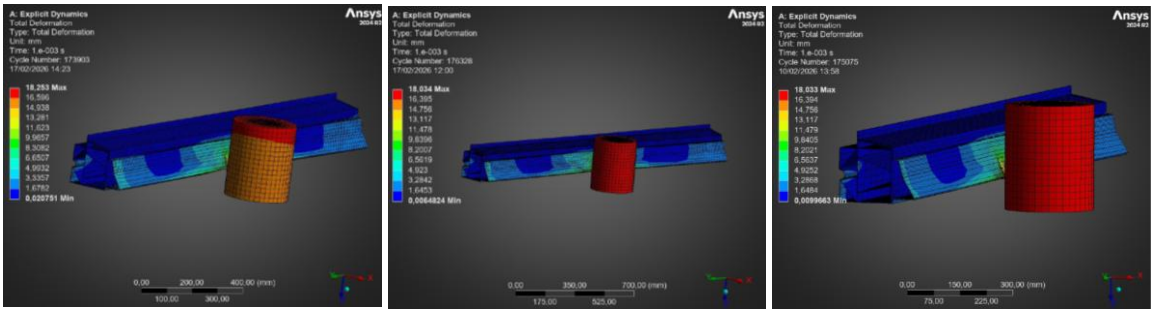

(a) (b) (c)

Figure 8. Comparison of total deformation distribution at 60 km/h: (a) Al 7075-T6, (b) Al 6082-T6, and (c) Al 6061-T6

Based on the simulation results in Figure 7, Al 7075-T6 exhibits a maximum deformation of approximately 18.253 mm, which is numerically slightly higher than that of the 6xxx series, which is in the range of 18.034 mm. However, this difference cannot be directly interpreted as an indication of poorer or better performance, as the magnitude of deformation in crashworthiness analysis must be related to the collapse mechanism and the stability of the structural response during the impact process. In the Al 7075-T6 material, the deformation occurs under more controlled active plastic conditions, characterized by the structure's ability to maintain a progressive folding pattern without exhibiting global instability. This means that although the deflection value is slightly larger, the response remains in the form of distributed deformation and does not cause sudden failure in the main structure.

Conversely, the 6xxx series exhibits nearly equivalent deformation values, indicating that the primary contribution to deformation control is more influenced by the multi-cell geometric configuration than by material characteristics alone. This geometry plays a crucial role in directing the collapse path so that impact energy can be gradually dissipated through a mechanism of repeated folding. As long as the deformation value remains below the critical intrusion threshold, the structure is deemed capable of maintaining the passenger safety zone during a lateral collision at 60 km/h. Therefore, performance evaluation is determined not only by the magnitude of deflection but also by deformation stability, consistent energy absorption, and the absence of penetration into the cabin zone.

Energy Absorption Efficiency

Energy absorption efficiency is a key indicator in evaluating crashworthiness performance, as it reflects the structure's ability to convert the kinetic energy resulting from an impact into internal deformation energy in a controlled manner. The simulation results in Figure 9 show the evolution of energy conversion during a 0.02-second impact duration, during which kinetic energy is gradually dissipated into internal energy within the side sill structure. The pattern of continuous internal energy increase without significant fluctuations indicates a stable numerical response and consistent material behavior during the deformation process. These conditions indicate that the structural collapse mechanism occurs progressively, so that there are no energy spikes typically associated with local instability or element failure. The trend of the curve also reflects the effectiveness of the multi-cell design in directing the deformation path, so that the energy absorption process occurs evenly in the plastic folding zone. Thus, the system is able to maintain a balance between energy dissipation and structural stability during the impact phase, which is a key characteristic in the design of passive safety structures.

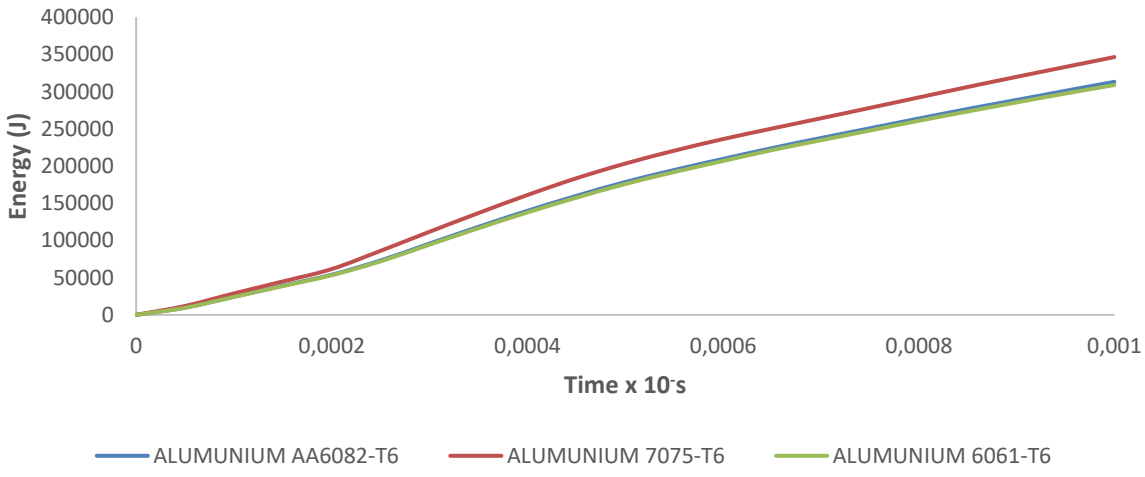

Figure 9. Energy absorber performance in side sill structure

The curve in Figure 9 shows a smooth and continuous increase in internal energy without any sharp fluctuations, indicating the stability of the numerical response and the consistency of the material's behavior during the impact process. This pattern suggests that the plastic deformation mechanism occurs in a controlled manner, in which kinetic energy is gradually converted into internal energy through a stable structural collapse process. In the material comparison results, Al 7075-T6 exhibits the highest energy absorption capacity with a value of approximately 3.46×10^5 Joules. However, this value cannot be interpreted in isolation as the sole indicator of material superiority; rather, it must be considered in conjunction with the accompanying deformation mechanisms, including fold stability, stress distribution, and the structure's ability to maintain integrity without global failure during dynamic loading.

These findings also confirm that the combination of multi-cell geometry and material characteristics with a high strength-to-mass ratio significantly contributes to the effectiveness of energy dissipation in side-impact structures. Geometry plays a role in directing the pattern of gradual collapse, while material properties determine the plastic capacity that can be mobilized during the impact process. Furthermore, the use of explicit dynamics simulations offers the advantage of capturing highly time-dependent transient material responses, including deformation evolution, energy distribution, and nonlinear contact interactions. This approach not only reduces reliance on costly and complex experimental testing, but also allows for a more detailed analysis of physical phenomena that are difficult to observe using conventional static methods.

Table 3. Crashworthiness parameters under side impact

Material	Deformation (mm)	Stress (MPa)	Yield Strength (MPa)	Energy (Joule)
6082-T6	18.034	262.64	276	3.13×10^5
7075-T6	18.253	499.84	260	3.46×10^5
6061-T6	18.033	250.69	503	3.09×10^5

A simulation of a side impact at 60 km/h shows that each material exhibits a different structural response, both in terms of deformation distribution and the stress intensity generated during the impact process. The data analysis reveals that deformation in the side sill tends to be localized in the area of direct contact with the rigid cylinder impactor, indicating that the damage mechanism is dominated by the impact zone without significant propagation to the surrounding structure. For the Al 7075-T6 material, the maximum deformation value recorded was approximately 18.253 mm [19]. Although numerically slightly higher than the 6xxx series, this condition should not be interpreted as a decline in performance, as the deformation that occurs remains within a stable progressive pattern. This means that the impact energy is absorbed through a controlled plastic mechanism without showing any signs of global failure in the main structure.

On the other hand, the von Mises stress value of approximately 499 MPa in Al 7075-T6 indicates that the material is operating near its yield point, allowing the impact energy to be effectively converted into plastic deformation. However, performance interpretation depends not only on the magnitude of the maximum stress but also on how that stress is distributed and accompanied by stable energy dissipation mechanisms. Overall, the difference in response between Al 7075-T6 and the 6xxx series reflects variations in plasticity characteristics and energy dissipation capabilities, rather than merely differences in the material's "strength" level [20]. A more comprehensive evaluation must still take into account deformation stability, progressive collapse patterns, and the structure's ability to maintain the integrity of the safety zone during the impact load.

CONCLUSIONS

Based on the results of numerical simulation and Finite Element Method (FEM)-based analysis of the side sill structure, several key conclusions can be drawn regarding its crashworthiness performance under lateral impact conditions. Overall, the material selection, structural configuration, and design parameters significantly influence the energy absorption capability and the ability of the structure to maintain cabin integrity.

From a material perspective, Aluminum 7075-T6 demonstrates the highest crashworthiness performance compared to Aluminum 6061-T6 and 6082-T6. Despite its slightly higher density, Aluminum 7075-T6 is able to withstand a maximum von Mises stress of 499.84 MPa and absorb internal energy up to 3.46×10^5 J. This indicates that the material operates near its yield limit under controlled plastic deformation conditions, allowing impact energy to be efficiently dissipated through progressive plastic deformation without causing global structural failure.

In terms of structural design, the multi-cell cross-sectional configuration of the side sill is highly effective in improving load distribution during impact events. This configuration enables the impact forces to be transferred through multiple deformation paths, preventing localized failure and promoting a more progressive collapse mechanism. This behavior is reflected in the stable deformation pattern observed at an impact velocity of 60 km/h,

where the maximum deformation remains controlled at approximately 18.253 mm. Such a response indicates that the structure is still capable of preserving the occupant survival space and minimizing intrusion into the cabin area.

Furthermore, the design parameter variation approach with a higher weighting assigned to energy absorption ($w_1 > w_2$) successfully produces a balanced structural configuration. Adjustments in wall thickness within critical regions of the side sill contribute to enhanced energy dissipation capacity without significantly increasing structural mass. This demonstrates that the proposed parametric variation strategy effectively improves crashworthiness performance while maintaining material efficiency.

Overall, the integration of Aluminum 7075-T6 with a multi-cell side sill structure provides a favorable solution for enhancing passive safety performance in vehicle side-impact scenarios. The combined approach ensures high energy absorption capability, stable deformation behavior, and effective preservation of cabin integrity under severe impact loading conditions.

REFERENCES

[1] D. L. Setyowati, Y. Setyaningsih, C. Suryawati, and D. Lestantyo, "Indonesian version of the motorcycle rider behaviour questionnaire: cross-cultural adaptation and validation," *Int. J. Public Heal. Sci.*, vol. 13, no. 3, pp. 1276–1285, 2024, doi: http://doi.org/10.11591/ijphs.v13i3.23837.

[2] C. Yuksel and C. O. Azeloglu, "Development and assessment of alternative designs for side impact beam," *Int. J. Crashworthiness*, vol. 29, no. 1, pp. 36–45, Jan. 2024, doi: https://doi.org/10.1080/13588265.2022.2153403.

[3] S. F. Abdulqadir and F. Tarlochan, "Composite Hat Structure Design for Vehicle Safety: Potential Application to B-Pillar and Door Intrusion Beam," *Materials*, vol. 15, no. 3. p. 1084, 2022. doi: https://doi.org/10.3390/ma15031084.

[4] R. Yang, S. Li, T. Cheng, P. Zou, and L. Tian, "Enhanced Side Pole Impact Protection: Crashworthiness Optimization for Electric Micro Commercial Vehicles," *Applied Sciences*, vol. 15, no. 4. p. 2220, 2025. doi: https://doi.org/10.3390/app15042220.

[5] A. Mortazavi Moghaddam, A. Kheradpisheh, and M. Asgari, "An integrated energy absorbing module for battery protection of electric vehicle under lateral pole impact," *Int. J. Crashworthiness*, vol. 28, no. 3, pp. 321–333, May 2023, doi: https://doi.org/10.1080/13588265.2022.2075123.

[6] A. Gashu and R. B. Nallamothu, "Improvement of crashworthiness of pickup vehicle for frontal and side collision using Finite Element analysis," *Adv. Mech. Eng.*, vol. 17, no. 2, pp. 1–16, 2025, doi: https://doi.org/10.1177/16878132251322029.

[7] A. Z. Yonatan, "Jumlah Mobil Listrik di Indonesia Naik." GoodStats, Apr. 07, 2026. [Online]. Available: https://data.goodstats.id/statistic/jumlah-mobil-listrik-di-indonesia-naik-ecNiK

[8] M. A. Akar, U. Kumlu, and Ş. Yıldızhan, "Numerical investigation of crash behavior of vehicle side door beams under high-speed pole side impacts," *Proc. Inst. Mech. Eng. Part D J. Automob. Eng.*, vol. 237, no. 14, pp. 3408–3418, Dec. 2023, doi: https://doi.org/10.1177/09544070221145523.

[9] U. N. E. C. for Europe, "ECE Regulation No. 135: Uniform Provisions Concerning the Approval of Vehicles with Regard to Their Pole Side Impact Performance." Apr. 08, 2026. [Online]. Available: https://unece.org/fileadmin/DAM/trans/main/wp29/wp29regs/2015/R135e.pdf

[10] National Highway Traffic Safety Administration, "Crash Simulation of FMVSS No. 214 Safety Performance," 2022.

[11] S. Ratnaparkhi, G. Shete, and R. Gummaraju, "Aluminium Sill Extrusions for Side-Pole Crashworthiness: A Review," *Int. J. Sci. Res. Publ.*, vol. 16, no. 2, 2026, doi: http://dx.doi.org/10.29322/IJSRP.16.02.2026.p17055.

[12] Marsono, M. R. Januarizki, M. L. Rasyad, E. Rachmadini, and G. A. Ghifari, "Pengujian Crashworthiness Honeycomb Sandwich Dengan Variasi Jumlah Lapisan Inti Menggunakan Software Ansys," *J. Rekayasa Energi dan Mek.*, vol. 3, no. 2, pp. 125–134, 2023, doi: https://doi.org/10.26760/JREM.v3i2.125.

[13] A. Thorat, S. Shinde, H. Patanwala, and E. Sahraei, "A Case Study on Crash Safety Strategies and Targets of Battery Electric VS Internal Combustion Engine Vehicles," in *2023 3rd International Conference on Electrical, Computer, Communications and Mechatronics Engineering (ICECCME)*, 2023, pp. 1–5. doi: https://doi.org/10.1109/ICECCME57830.2023.10253086.

[14] H. Zainuddin, M. B. Ali, K. A. Zakaria, L. H. Paijan, M. F. Mamat, and M. H. Abu Bakar, "Investigation of Impact Properties under Instrumented Charpy Test," *J. Eng. Technol. Sci.*, vol. 56, no. 3, pp. 329–339, Jun. 2024, doi: https://doi.org/10.5614/j.eng.technol.sci.2024.56.3.2.

[15] T. Ye *et al.*, "High-Temperature Tensile Mechanical Properties and Microstructure of Rolled 6082-T6 Aluminum Alloy Sheets," *Materials*, vol. 16, no. 21. p. 7019, 2023. doi: https://doi.org/10.3390/ma16217019.

[16] J. A. Frutos, R. R. Ambriz, C. J. García, and D. Jaramillo, "Orthogonal impact load in 6061-T651 and 7075-T651 aluminum alloy plates," *J. Mater. Res. Technol.*, vol. 26, pp. 4245–4262, 2023, doi: https://doi.org/10.1016/j.jmrt.2023.08.174.

[17] M. S. Lee and Y. H. Moon, "Collision Resistance of a Lightweight Center Pillar Made of AA7075-T6," *Int. J. Automot. Technol.*, vol. 22, no. 4, pp. 853–862, 2021, doi: https://doi.org/10.1007/s12239-021-0077-4.

[18] B. K. Yadav, M. Jahangiri, and D. Singh, "Experimental and Numerical Simulation to Validate Critical Perforation Velocity on a Flat Plate Aluminium Alloy 6061," *Adv. Mater. Sci. Eng.*, vol. 2022, no. 1, p. 3707200, Jan. 2022, doi: https://doi.org/10.1155/2022/3707200.

[19] S.-W. Byun, Y.-J. Joo, S.-Y. Lee, and S.-W. Kim, "Experimental and Numerical Study on the Perforation Behavior of an Aluminum 6061-T6 Cylindrical Shell," *Materials*, vol. 16, no. 21. p. 7055, 2023. doi: https://doi.org/10.3390/ma16217055.

[20] E. E. Aytimur, "Crashworthiness Simulations with LS-DYNA Investigating the Effect of Strain Rate-Dependent Material Models," *Procedia Struct. Integr.*, vol. 68, pp. 540–546, 2025, doi: https://doi.org/10.1016/j.prostr.2025.06.094.

[21] A. Shokry, S. Gowid, H. Mulki, and G. Kharmanda, "On the Prediction of the Flow Behavior of Metals and Alloys at a Wide Range of Temperatures and Strain Rates Using Johnson–Cook and Modified Johnson–Cook-Based Models: A Review," *Materials*, vol. 16, no. 4. p. 1574, 2023. doi: https://doi.org/10.3390/ma16041574.

[22] V. Kumar Reddy Sirigiri, V. Yadav Gudiga, U. Shankar Gattu, G. Suneesh, and K. Mohan Buddaraju, "A review on Johnson Cook material model," *Mater. Today Proc.*, vol. 62, pp. 3450–3456, 2022, doi: https://doi.org/10.1016/j.matpr.2022.04.279.

[23] A. R. Prabowo *et al.*, "Comparative study of shell element formulations as NLFE parameters to forecast structural crashworthiness," vol. 10, no. 1, 2023, doi: https://doi.org/10.1515/cls-2022-0217.

[24] B. Ponnusamy, "High-fidelity numerical framework for crashworthiness evaluation of passenger car body structures under full-frontal impact," *Sci. Rep.*, vol. 16, no. 1, p. 10563, 2026, doi: https://doi.org/10.1038/s41598-026-43474-z.

[25] C. Parenteau, B. N. Ault, D. Toomey, R. Krishnaswami, and R. Burnett, "Side Impact Characteristics in Modern Light Vehicles," in *WCX SAE World Congress Experience*, SAE International, Apr. 2024. doi: https://doi.org/10.4271/2024-01-2646.

[26] S. Jonsson and J. Kajberg, "Evaluation of Crashworthiness Using High-Speed Imaging, 3D Digital Image Correlation, and Finite Element Analysis," *Metals*, vol. 13, no. 11. p. 1834, 2023. doi: https://doi.org/10.3390/met13111834.